Electric double layer interactions in bacterial adhesion to surfaces

Albert T. Poortinga[a], Rolf Bos[a], Willem Norde[a,b], Henk J. Busscher[a]

[a]*Department of Biomedical Engineering, University of Groningen, Antonius Deusinglaan 1, 9713 AV Groningen, The Netherlands*

[b]*Laboratory of Physical Chemistry and Colloid Science, Wageningen University, Dreijenplein 6, 6703 HB Wageningen, The Netherlands*

ELSEVIER

Amsterdam–London–New York–Oxford–Paris–Shannon–Tokyo

Contents

ELSEVIER

Surface Science Reports 47 (2002) 1–32

surface science reports

www.elsevier.com/locate/surfrep

Electric double layer interactions in bacterial adhesion to surfaces

Albert T. Poortinga[a,1], Rolf Bos[a,1], Willem Norde[a,b], Henk J. Busscher[a,*]

[a]*Department of Biomedical Engineering, University of Groningen, Antonius Deusinglaan 1, 9713 AV Groningen, The Netherlands*

[b]*Laboratory of Physical Chemistry and Colloid Science, Wageningen University, Dreijenplein 6, 6703 HB Wageningen, The Netherlands*

Manuscript received in final form 8 January 2002

Abstract

The DLVO (Derjaguin, Landau, Verwey, Overbeek) theory was originally developed to describe interactions between non-biological lyophobic colloids such as polystyrene particles, but is also used to describe bacterial adhesion to surfaces. Despite the differences between the surface of bacteria and that of non-biological particles, DLVO-descriptions of bacterial adhesion have nearly always treated bacteria as if they were non-biological particles and consequently in many cases these descriptions have failed to describe bacterial adhesion adequately. This review summarizes recent advances in colloid and surface science regarding the electrokinetic characterization of biological colloids, most notably bacteria, and their electric double layer interactions with surfaces.

Keywords: Bacterial adhesion; Electrostatic interactions; DLVO theory; Ion-penetrability; Electrophoretic mobility; Charge-regulation

1. Introduction

Adhesion of colloidal particles may be described by the DLVO (Derjaguin, Landau, Verwey, Overbeek) theory. According to this theory, particle adhesion is governed by long-range interactions between the adhering particle and the macroscopic substratum surface. These interactions include Lifshitz–van der Waals interactions and interactions resulting from overlapping electric double layers (also referred to as electrostatic interactions). The two types of interactions are assumed to be additive

* Corresponding author. Tel.: +31-50-3633140; fax: +31-50-3633159.
E-mail address: h.j.busscher@med.rug.nl (H.J. Busscher).
[1] Present address: Friesland Coberco Dairy Foods, Corporate Research, Harderwijkerstraat 41006, 7418 BA Deventer, The Netherlands.

0167-5729/02/$ – see front matter
PII: S0167-5729(02)00032-8

allowing the total Gibbs energy of adhesion to be expressed as a function of the distance between the particle and the macroscopic substratum surface. Recently [1], the so-called XDLVO theory has been forwarded, which in addition to classical DLVO interactions, accounts for short-range Lewis acid–base or hydration interactions. The DLVO theory has also been applied to describe bacterial adhesion[2] [3–5] in a wide range of applications, involving microbial adhesion on food processing equipment [6,7], biomaterials implants [8], surfaces in the oral cavity [9], on grains of sand [10] and on bioreactor supports [11,12]. Also, the DLVO theory has been used to describe the stability of bacteria in suspension [13].

The bacterial cell surface carries a net negative charge under most physiological conditions, with a few exceptions [14,15]. As most natural surfaces are negatively charged as well, bacteria generally experience electric double layer repulsion when approaching these surfaces. Experimental studies have shown the importance of electric double layer interactions in bacterial adhesion [16–19], but have also revealed discrepancies between observations and theoretical expectations, some of which are reviewed in Table 1.

The bacterial cell surface is a highly dynamic surface responding strongly to environmental changes through adsorption of ions and macromolecular components. Charged groups may associate or dissociate upon changes in pH or ionic strength of the suspending fluid, but also upon approach of a charged surface, either of another bacterium or a substratum. This, in addition, may induce changes in the conformation of different kinds of surface appendages, such as fibrils, fimbriae or flagellae [28]. Moreover, the bacterial cell surface may be penetrable to solvents and solutes, in particular ions, either due to the presence of a peptidoglycan layer [29,30] as on Gram-positive bacteria, the presence of surface appendages [31] or a slime capsule [32]. Inside the bacterial cell wall, charged groups are present and the distribution of these charges influences electric double layer interactions in bacterial adhesion [29,32], unlike for many synthetic colloids for which the electric charges in the plane of the outer surface determines their interaction with other surfaces.

Summarizing, the bacterial cell wall is structurally and chemically more complex and heterogeneous than the surface of synthetic colloidal particles and this has an impact on bacterial adhesion to surfaces. Yang et al. [33] have shown, for instance, that adhesion of polystyrene particles is not an appropriate model for bacterial adhesion because of differences in surface structure between bacteria and polystyrene particles. In an attempt to account for the presence of polymeric structures on bacterial cell surfaces, steric interactions have been introduced in addition to DLVO interactions [16,26,27,34]. However, little attention has been paid to the effect of the bacterial cell surface structure on DLVO interactions and as far as electric double layer interactions are concerned, bacteria have mostly been treated as model colloidal particles [2,3].

The electric potential at the bacterial cell surface is usually inferred from measured electrophoretic mobilities, i.e. the velocity of suspended bacteria in an aqueous phase under the influence of an applied electric field. Derivation of the bacterial cell surface potential from the electrophoretic mobility is not straightforward and strongly depends on the model used to describe the cell surface. Bacterial cell surfaces have hitherto in most cases been modeled as ion-impenetrable and non-conducting [35], but this simplification neglects effects of surface conductivity [29] and of penetrability of the bacterial cell surface to fluid flow [31,36]. Apart from influencing the electrophoretic mobility, penetrability of the

[2] See, for example [2] for a review comprising 266 references.

Table 1
Representative examples of deviations from the DLVO or XDLVO theory observed in bacterial adhesion studies

Strains	Experiment	Findings	Reference
Arthrobacter, *Corynebacterium*, *Rhodococcus*, *Pseudomonas*, *Gordona*	Adhesion to glass and Teflon	Experimentally obtained energy barriers towards adhesion are orders of magnitude smaller than DLVO predictions at low ionic strength	[16]
E. coli	Adhesion to sludge flocs	Adhesion does not correlate with bacterial zeta potential but with the fraction of positive charges present on the bacterial cell surface	[20]
Vibrio alginolyticus	Adhesion to hydroxyapatite	Bacterial adhesion increases at increasing ionic strength, in accordance with DLVO theory, but decreases when ionic strength exceeds 0.1 M	[21]
Corynebacterium	Accumulation of bacteria at an air–water interface	In contrast to DLVO predictions under repulsive conditions, accumulation decreases for increasing ionic strength	[22]
S. salivarius	Adhesion to glass	Despite small differences in DLVO interaction energies, adhesion rates of a fibrillated and non-fibrillated strain differ strongly	[18]
Marine strains	Adhesion to hydrophobic and hydrophilic polystyrene	No correlation between adhesion and ionic strength exists	[23]
Sphingomonas paucimobilis	Adhesion to bare glass and EPS coated glass	XDLVO theory can explain adhesion to glass, but cannot explain adhesion to glass coated with bacterial EPS	[24]
Pseudomonas	Adhesion to sand	A fraction of the bacteria adheres faster than the rest, while DLVO calculations predict no difference	[25]
E. coli	Direct measurement of bacterial interaction force with glass, mica and hydrophobic polymers	Force measurements do not correlated with XDLVO calculations for a lipopolysaccharide covered strain, but do correlate for a strain with truncated lipopolysaccharide chain	[26]
Pseudomonas, *Burkholderia*	Measurement of bacterial interaction with silicon nitride AFM tip	A repulsive force extending over longer distances (>100 nm) than predicted by DLVO theory is measured	[27]

bacterial cell wall is also expected to influence electric double layer interactions in bacterial adhesion to surfaces [32,37].

The aim of this paper is to summarize recent advances in colloid and surface science regarding electric double layer interactions, which help better to understand mechanisms of bacterial adhesion. To this end, first a description is given of bacterial cell surfaces as compared with the surface of model colloidal particles. Second, the impact of specific characteristics of bacteria on their electrochemical properties and their electric double layer interactions with surfaces as follows from the DLVO theory, is discussed in relation to existing literature on bacterial adhesion.

2. Electrochemistry of the bacterial cell surface

It is considered outside the scope of this paper to provide a detailed review on bacterial cell surfaces (see, for example [38] or [28]), but for full comprehension some important features of bacterial cell surfaces as compared with model colloidal particles will be briefly presented.

2.1. Structure of the bacterial cell surface

The definition of a surface as a two-dimensional structure does not hold for bacterial cell walls. Consequently, we will distinguish a three-dimensional bacterial cell wall including all structures on top of it and denote all outermost components as the bacterial cell surface.

Bacterial strains are either Gram-positive or Gram-negative, as can be distinguished by Gram-staining [38]. The compositions of the cell wall of Gram-positive and Gram-negative bacteria differ considerably. The cell wall of Gram-positive bacteria consists of a 15–80 nm thick rigid layer of peptidoglycan on top of the phospholipid rich cytoplasmic membrane (see Fig. 1). The density of the peptidoglycan layer varies throughout the layer with an estimated average density of about 20% (w/v) [39]. The cell wall of Gram-negative bacteria consists of a much thinner peptidoglycan layer of 1–2 nm thickness sandwiched between two phospholipid bilayer membranes: the inner, cytoplasmic membrane and an outer membrane (see also Fig. 1). The outer membrane contains pores, formed by aggregates of proteins, which facilitate the selective transport of molecules through the membrane. Because selectively transported molecules include charged species, they give rise to a potential difference across

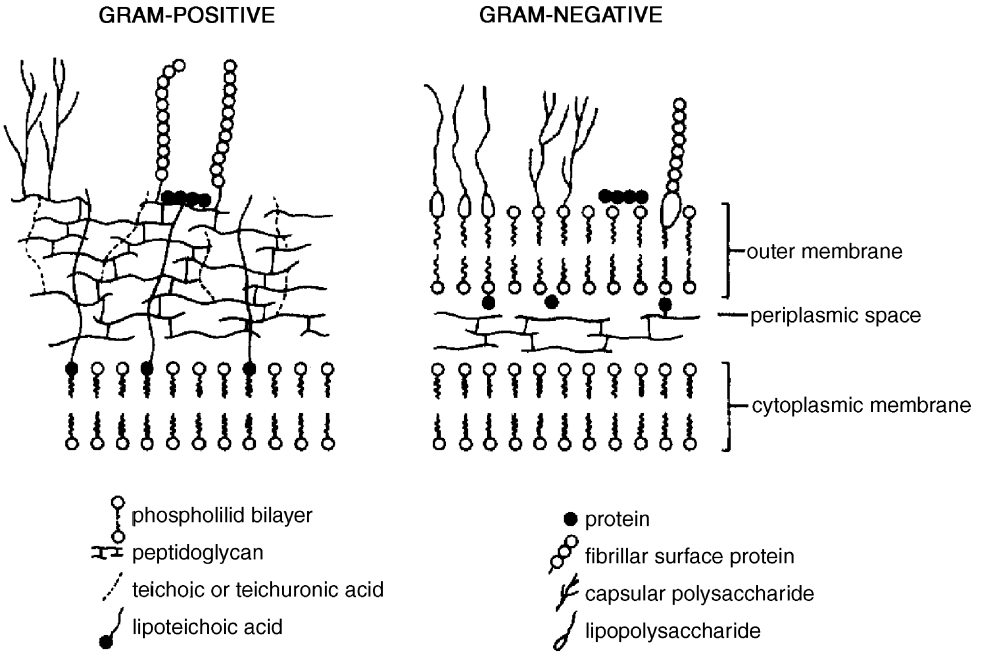

Fig. 1. Generalized, schematic representation of the Gram-positive and Gram-negative cell surface showing possible arrangement of polymers (not drawn to scale).

the membrane, the transmembrane potential [40]. An inventory of the pH dependencies of the zeta potentials of nearly 100 different bacterial strains, has not shown a systematic difference between Gram-positive and Gram-negative strains [41].

A variety of chemical heterogeneities and structural features can be found on top of the peptidoglycan layer in Gram-positive or on top of the outer membrane in Gram-negative bacteria, which constitute the outermost cell surface. Structural surface appendages can be visualized by electron microscopy after negative-staining and include flagellae, fimbriae, fibrils and other types of molecular surface structures. Flagellae are involved in cell motility and are composed of several polypeptides forming a filament (about 20 nm in diameter and 10–20 μm in length), a hook and a basal body. Fimbriae (see Fig. 2a) are proteinaceous appendages, 0.2–2.0 μm in length and 2–10 nm in diameter, with a high content of hydrophobic amino acid residues. Fimbriae can be either rigid or flexible. Fibrils are shorter than fimbriae, usually less than 0.2 μm in length, and do not have a measurable width as they clump together after staining, as can be seen in Fig. 2b. Bacteria may carry fibrils with different lengths and fibrils may be distributed either homogeneously (''peritrichously'', see Fig. 2c) or heterogeneously (''tufted'', see Fig. 2b) over the surface [41]. Interestingly, bacterial strains that depend heavily on their ability to adhere to surfaces for their survival, such as oral bacteria adhering to tooth surfaces in order to prevent being swallowed, mostly carry fibrils or fimbriae, which consequently have been associated with bacterial adhesion [42]. Many bacterial strains excrete polymeric substances, referred to as extracellular polymeric substances (EPS), consisting of polysaccharides, glycoproteins, lypopolysaccharides and uronic acids [43]. The EPS may form a capsule around bacteria, with a thickness of up to 200 nm (Fig. 2d). When the EPS is loosely associated with the bacterial cell surface, it is mostly referred to as a slime layer. Capsules are very tenuous and their water content may be as high as 98% (w/v) [44]. Surface-arrays (or S-arrays) are assemblies of glycoproteins, non-covalently attached to the bacterial surface that form regularly structured arrays with pore diameters in the range of 10 nm [45] (see Fig. 2), therewith acting as permeability barriers for macromolecules.

In conclusion, the bacterial cell surface is highly complex and differs strongly from the surface of non-biological colloids, such as polystyrene particles (compare Fig. 2f). As the great majority of bacterial cell surface components in water are charged due to dissociation from or association with protons, bacteria may be regarded as charged colloidal 'particles'.

2.2. The electric double layer at bacterial cell surfaces

Bacterial cell surface charge originates from dissociation or protonation of carboxyl, phosphate and amino groups and consequently depends on pH. Possible chemical reactions charging the bacterial cell surface are given in Table 2 together with their estimated intrinsic dissociation constants K_a [30,46]. It should be noted that the effective dissociation constants as valid for bacterial cell surface groups also depend on environmental properties, such as the local hydrophobicity and electric potential [30]. At physiological pH values, i.e. between 5 and 7, most bacterial strains are negatively charged, as the number of carboxyl and phosphate groups exceeds the number of amino groups. Hitherto a net positive surface charge at physiological pH values has only been reported for two bacterial isolates, viz. a *Streptococcus thermophilus* and *Stenotrophomonas maltophilia* strain [14,15].

A bacterial cell surface with N_1 acid (such as –COOH) and N_2 base (such as $-NH_2$) uncharged groups per unit volume with dissociation constants K_{a1} and K_{a2} has a space charge density fixed to the bacterial

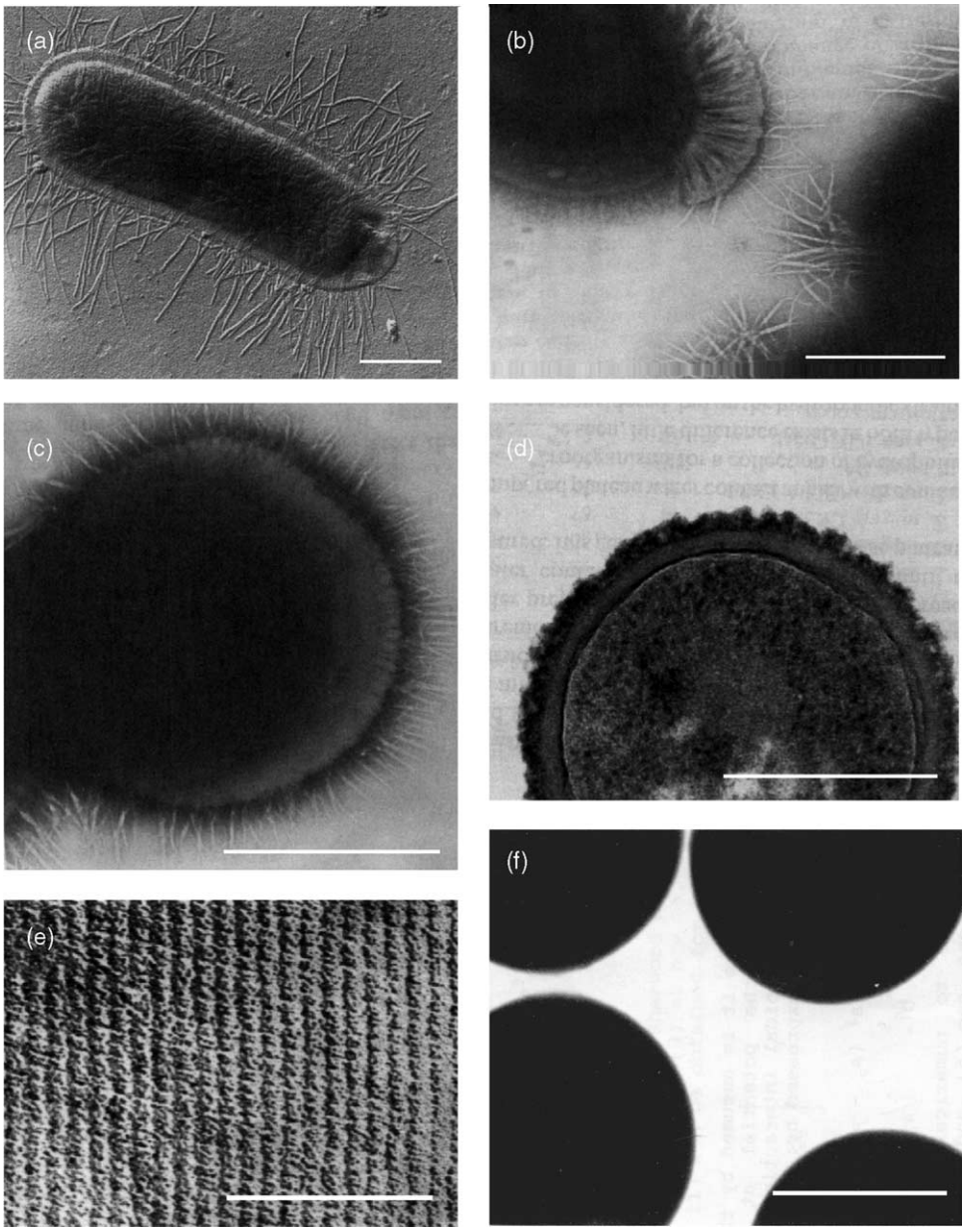

Fig. 2. Electron micrographs of possible bacterial cell surface structures (a)–(e) and of the surface of polystyrene particles (f). Bar denotes 0.5 μm, except for (e) where it denotes 0.1 μm: (a) *E. coli* cell with rigid, peritrichous fimbriae, about 7 nm in diameter and up to 1 μm long. Taken from Busscher et al. [41]. (b) *Streptococcus oralis* CN3410 showing lateral fibrillar tufts of both lengths, long (289 nm) and short (159 nm) fibrils, as well as a peritrichous 'fuzz' all over the cell surface. One tuft shows two lengths of fibrils, while the other tufts show one length of fibrils in the same population of cells. Taken from Busscher et al. [41]. (c) *S. salivarius* CN3928 showing peritrichously arranged, clumped fibrils with a length of 191 nm. Taken from Busscher et al. [41]. (d) *Lactobacillus lactis* RC14 surrounded by a thick, ruthenium red/uranyl acetate-stainable layer with no obvious surface appendages. Taken from Busscher et al. [41]. (e) S-layer present on *Bacillus stearothermophilus* NRS2004. Taken from Hancock [28]. (f) Polystyrene particles. Taken from Sjollema and Busscher [42].

Table 2
Ionizable surface groups in various molecular species that may be present on bacterial cell surfaces and the $-\log_{10}$ value of their dissociation constants (pK_a). Data compiled from Rijnaarts et al. [46] and van der Wal et al. [30]

Reaction	Molecule	pK_a
$-COOH \Leftrightarrow -COO^- + H^+$	Polysaccharide	2.8
	Protein, peptidoglycan	Between 4.0 and 5.0
$-NH_3^+ \Leftrightarrow -NH_2 + H^+$	Protein, peptidoglycan	Between 9.0 and 9.8
$-HPO_4 \Leftrightarrow -PO_4^- + H^+$	Teichoic acids	2.1
$-H_2PO_4 \Leftrightarrow -HPO_4^- + H^+$	Phospholipids	2.1
$-HPO_4^- \Leftrightarrow -PO_4^{2-} + H^+$	Phospholipids	7.2

cell surface that is determined by the dissociation/association equilibria of the acid/base groups, as described by the ionizable surface group model [47]

$$\rho_{\text{fix}} = eN_1 \frac{-K_{\text{a1}}}{K_{\text{a1}} + [\text{H}^+]\exp(-e\psi/kT)} + eN_2 \frac{[\text{H}^+]\exp(-e\psi/kT)}{K_{\text{a2}} + [\text{H}^+]\exp(-e\psi/kT)} \tag{1}$$

with e is the electron charge, k the Boltzmann constant, T the absolute temperature, $[H^+]$ the proton concentration and ψ the electric potential at the position of the ionizable surface group. The degree of ionization depends on the electric potential, because the local proton activity is a function of the local electric potential via Boltzmann's law.

Fig. 3a schematically shows the distribution of ions and the electric potential near a charged bacterial cell surface in contact with a solution according to the Stern–Grahame model [48]. The bacterium is described as an ion-impenetrable particle with its charge concentrated and smeared out solely at the outer surface. Closest to the surface ions reside that are subject to an attractive non-electrostatic interaction potential, i.e. these ions are specifically adsorbed and, as a consequence, have lost part of their hydration water. The finite size of the adsorbed ions keeps them at a certain distance (at what is called the inner Helmholtz plane) from the surface, yielding a region adjacent to the surface that is free of charge. The amount of specifically adsorbed charge per unit area can be expressed using a modified Langmuir isotherm [48,49]

$$\sigma_{\text{ads}} = \frac{zeCN_{\text{ads}}\exp(-\Delta_{\text{ads}}G/kT)}{1 + C\exp(-\Delta_{\text{ads}}G/kT)} \tag{2}$$

in which $\Delta_{\text{ads}}G$ is the Gibbs energy of adsorption per molecule according to

$$\Delta_{\text{ads}}G = ze\psi + \Delta_{\text{spec}}G, \tag{3}$$

where $ze\psi$ represents the electrostatic interaction energy and $\Delta_{\text{spec}}G$ is the Gibbs energy of specific interaction. N_{ads} denotes the number of adsorption sites per unit area. C and z denote the bulk concentration and the valency of specifically adsorbing ions, respectively. Specific adsorption of ions is an important source of bacterial surface charge and especially multivalent cations such as Ca^{2+} are known to specifically adsorb [49–51]. The electric potential profile at the bacterial surface is governed by the Poisson equation, which for a flat geometry reads

$$\frac{\text{d}^2\psi(x)}{\text{d}x^2} = -\frac{\rho(x)}{\varepsilon} \tag{4}$$

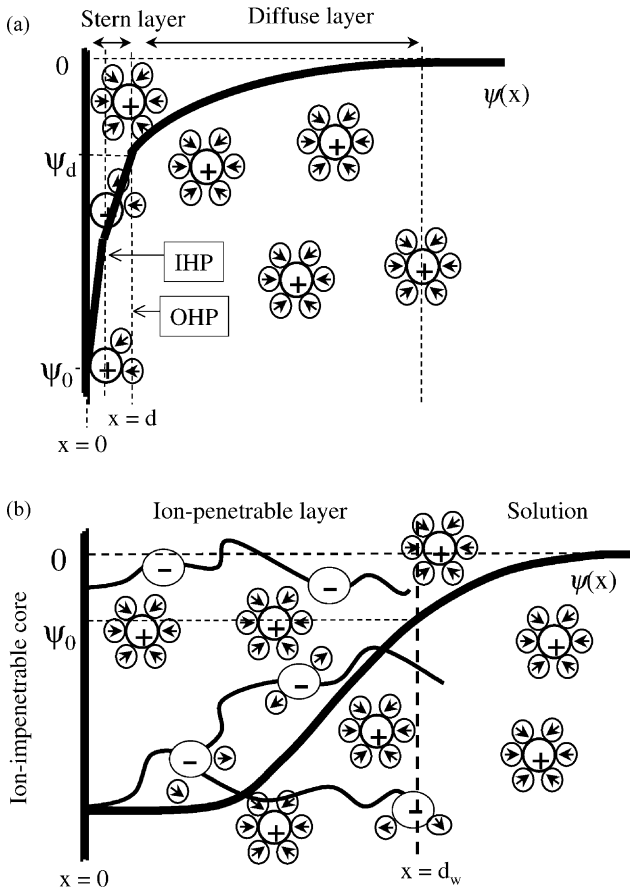

Fig. 3. The electric double layer at a negatively charged ion-impenetrable (a) and ion-penetrable bacterium (b). IHP is the inner Helmholtz plane, while OHP represents the outer Helmholtz plane. Circles denote ions fixed to the surface structures constituting the ion-penetrable layer (minus sign) or ions in solution (plus sign), while circles marked with an arrow indicate water dipoles (arrow points toward oxygen). Drawn line schematically gives the electric potential profile $\psi(x)$ with ψ_0 and ψ_d the electric potential at the bacterial surface and across the diffuse double layer, respectively.

with ρ the space charge density and ε the dielectric permittivity in the solution. In solution the space charge is constituted by ions and hence

$$\rho(x) = eN_A \sum_i z_i c_i(x) \tag{5}$$

with N_A the Avogadro's number, z_i the valencies and c_i the concentration of the various ionic species denoted by i. Ions in solution that do not specifically interact with the surface are hydrated and therefore cannot approach the surface any closer than the outer Helmholtz plane (see Fig. 3a). In thermodynamic equilibrium, the ion concentration in the region beyond the Helmholtz plane follows the Boltzmann distribution:

$$c_i(x) = c_{\text{bulk},i} \exp\left(-\frac{z_i e\psi(x)}{kT}\right). \tag{6}$$

The charge density constituted by these ions is referred to as the diffuse double layer charge ρ_{el}. Eqs. (4)–(6) can be combined to yield a differential equation describing the electric potential profile, known as the Poisson–Boltzmann equation. Assuming a low electric potential, such that $|ze\psi/kT| < 1$ (which for a 1-1 electrolyte corresponds to $|\psi| \leq 25$ mV), the Poisson–Boltzmann equation may be linearized and solved to give [52]

$$\psi(x) = \psi_d \exp(-\kappa(x-d)) \tag{7}$$

in which the potential ψ_d is the potential difference across the diffuse part of the double layer, which is related to the surface charge density σ_d in the diffuse part of the double layer charge through

$$\sigma_d = \varepsilon\kappa\psi_d, \tag{8}$$

where $\varepsilon\kappa$ is the diffuse double layer capacitance. The diffuse double layer thickness κ is determined by the ionic composition of the solution through

$$\kappa = \sqrt{\frac{e^2\sum_{i=1}^{N} c_{bulk,i} z_i^2}{\varepsilon kT}} \tag{9}$$

for a solution containing N different ionic species. The inner and outer Helmholtz regions also have a certain capacitance and the total electric capacitance of the bacterial cell surface can be described as the capacitances of the inner and outer Helmholtz layers and the diffuse double layer in series.

The foregoing description of the bacterial cell surface assumes that the surface charge is concentrated at an infinitesimally thin layer. From Fig. 1, it can be readily seen that this assumption is invalid for a bacterial cell surface [53] and that bacteria will have their surface charge distributed over a three-dimensional surface layer of finite thickness, which is ion-penetrable. van der Wal et al. [30], using proton titration, deduced surface charges ranging from -20 to -50 μC/cm^2 in 1 mM KNO_3 for several Gram-positive bacteria including Coryneforms, Rhodococci and Bacillus isolates. It was concluded that this charge could not be accommodated in an infinitesimally thin surface layer, as this would yield a double layer potential of several volts. Instead, it was argued that this charge would be distributed over an ion-penetrable layer of around 50 nm thickness, corresponding with the thickness of the bacterial peptidoglycan layer.

The essential differences between an ion-impenetrable and an ion-penetrable bacterial surface can be seen by comparing Fig. 3a and b. As ions can penetrate the surface no Stern layer exists at an ion-penetrable surface. Also, counter ions partly screen the fixed charges inside the ion-penetrable layer. In order to describe the electric potential distribution inside an ion-penetrable layer, Eq. (4) is re-written as [54]

$$\frac{d^2\psi(x)}{dx^2} = -\frac{\rho_{fix}(x) + \rho_{el}(x)}{\varepsilon_w} \tag{10}$$

with $\rho_{fix}(x)$ the fixed charge density resulting from the charged groups of the surface structures constituting the ion-penetrable layer (the term fixed is used to distinguish these charges from the diffuse double layer charges), $\rho_{el}(x)$ the charge density constituted by diffusely distributed ions that have penetrated the ion-penetrable layer and ε_w the dielectric permittivity inside the ion-penetrable layer. In principle, in addition to $\rho_{fix}(x)$ and $\rho_{el}(x)$ a specifically adsorbed charge density may also be present inside the ion-penetrable layer, but this is neglected here. Inside the solution no fixed charge density

exists and Eq. (4) holds, while furthermore a number of boundary conditions apply

$$\varepsilon_w \frac{d\psi}{dx}\bigg|_{x=0} = -\sigma_0, \tag{11}$$

$$\psi(x \downarrow d_w) = \psi(x \uparrow d_w), \tag{12}$$

$$\varepsilon_w \frac{d\psi}{dx}(x \uparrow d_w) = \varepsilon \frac{d\psi}{dx}(x \downarrow d_w) \tag{13}$$

with σ_0 the surface charge density at the ion-impenetrable core which is usually assumed to be zero. In the following it is assumed that the dielectric permittivities in and outside the ion-penetrable layer are identical. This approximation has been made before, as the bacterial ion-penetrable layer mainly consists of water. However, it may be reasonable to use lower values for the dielectric permittivity because water is immobilized in a gel-like structure to a certain extent. Eqs. (4) and (10)–(13) determine the potential distribution in the interfacial region of an ion-penetrable bacterial cell surface. Analytical results have been obtained under various simplifying conditions, such as the assumptions of low potential, a uniform fixed charge density and an infinitely thick ion-penetrable layer [54]. The last assumption is valid when the ion-penetrable layer thickness exceeds the diffuse double layer thickness several times, as usually holds for bacteria. Fig. 4 gives examples of the electric potential distribution at an ion-penetrable interface with a uniform fixed charge density. Far inside the ion-penetrable layer a constant potential, the so-called Donnan potential ψ_{DON} is reached

$$\psi_{DON} = \frac{\rho_{fix}}{\varepsilon \kappa^2}. \tag{14}$$

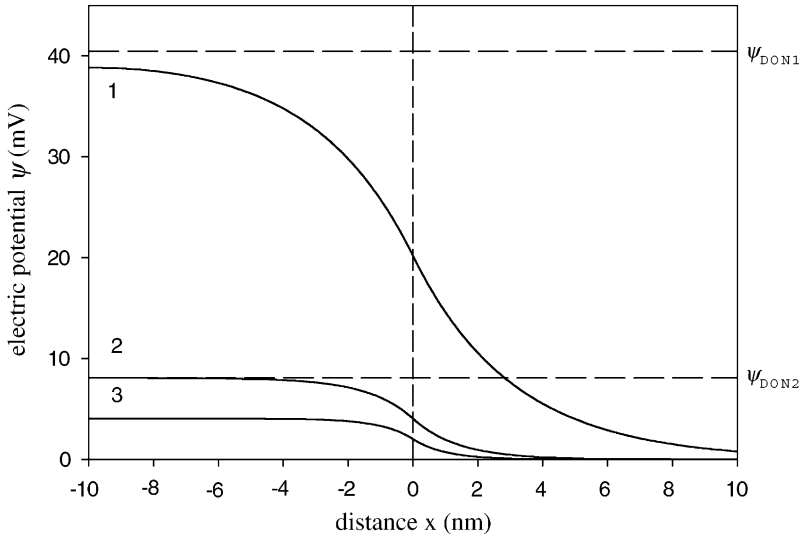

Fig. 4. Potential distribution in a 1-1 electrolyte solution with different molarities across a uniformly charged ion-penetrable surface layer calculated using the linearized Poisson–Boltzmann equation [61] using a fixed charge density of 3×10^6 C/m^3, dielectric permittivity inside the ion-penetrable layer and the solution of $80\varepsilon_0$, temperature $T = 298$ K. Curve 1: molarity of 0.01 M; curve 2: 0.05 M; curve 3: 0.1 M. Donnan potentials for curve 1 (ψ_{DON1}) and 2 (ψ_{DON2}) are indicated by the dashed lines.

At the location of the Donnan potential, the fixed charge density is fully compensated by the local diffuse charge density.

Bacterial ion-penetrable layers have been associated with appendages [31,55] or capsules [32] present at the bacterial cell wall or with peptidoglycan layers in the cell wall of Gram-positive bacteria [29,36], although also the electrophoretic mobility of the Gram-negative *Escherichia coli* has been be successfully described by assuming the cell surface to be ion-penetrable [36].

2.3. Characterization of bacterial cell surface charge

Methods to determine bacterial cell surface charge include particulate micro-electrophoresis, proton titration and dielectric spectroscopy. Proton titration involves adding protons to a bacterial suspension while monitoring the pH [30]. The charge of the bacterial cells is then obtained from the amount of protons reacting with the bacterial cell surface. In dielectric spectroscopy [56], the frequency dependence of the complex conductivity of a bacterial suspension is measured, from which information on the electric double layer of bacteria can be derived. Particulate micro-electrophoresis reveals the electrokinetic potential (zeta potential) and electrokinetic charge of the bacteria and is by far the most frequently used method. Therefore, we will only discuss this method.

2.3.1. Particulate micro-electrophoresis

During particulate micro-electrophoresis, the velocity u_E of bacteria suspended in an aqueous medium, as acquired under the influence of an applied electric field E (usually in the range 100–1000 V/m), is measured by microscopic observation [57] to yield the electrophoretic mobility

$$\mu = \frac{u_E}{E}. \tag{15}$$

For a particle with radius a and high ionic strengths, i.e. when $\kappa a \gg 1$, the electrophoretic mobility is related to the zeta potential ζ by the Helmholtz–Von Smoluchowski equation [58]

$$\mu = \frac{\varepsilon}{\eta}\zeta \tag{16}$$

with ε the dielectric permittivity and η the bulk viscosity of the suspending solution. The zeta potential is defined as the electric potential at the hydrodynamic plane of shear or, otherwise called, the slip plane. The slip plane is the hypothetical interface between a stagnant liquid layer adjacent to the particle surface and the liquid moving relative to the surface during electrophoresis. The slip plane is generally assumed to be located within several nanometers of the particle surface [59]. For bacteria, however, it is difficult to define the location of the surface, and consequently of the slip plane, due to the inherent morphological heterogeneity of their surface.

The zeta potential is often assumed to be equal to the diffuse double layer potential ψ_d. The net charge density of the bacterial surface, including the Stern layer, equals the diffuse double layer charge and in most cases does not exceed 3×10^{-2} C/m^2 [59]. On the basis of this maximum charge density, Busscher and Norde [60], applying Eq. (8), calculated a theoretical limit for bacterial zeta potentials which is presented as a function of ionic strength in Fig. 5. An extensive inventory of 96 different bacterial strains and species, showed that all bacterial zeta potentials were within this theoretical upper limit [41].

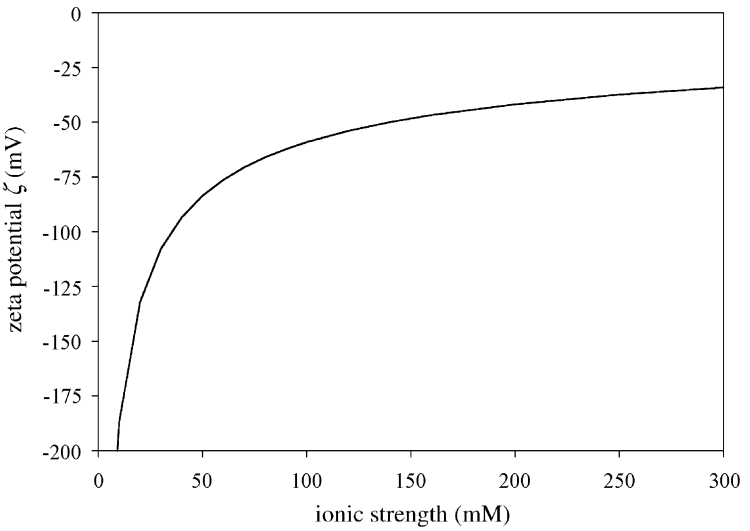

Fig. 5. Theoretical upper limit for the bacterial zeta potential as a function of ionic strength [60] assuming the zeta potential to be equal to the diffuse double layer potential and assuming a diffuse double layer charge of 3×10^{-2} C/m^2 (see Eq. (8)).

Fig. 6 shows the electrophoretic mobility as a function of ionic strength for a bacterium covered with a 50 nm thick ion-penetrable layer according to the Helmholtz–Von Smoluchowski relation, assuming the zeta potential to coincide with the potential at the ion-penetrable surface (see curve 1). Although the great majority of electrokinetic studies of bacteria applies the Helmholtz–Von Smoluchowski relation, use of this relation is incorrect in several cases. First, electrophoresis polarizes the double layer around bacteria creating a dipole moment that opposes the applied electric field. Double layer polarization mainly affects bacterial electrophoretic mobilities at low ionic strengths, when $\kappa a \gg 1$ is no longer valid [29] (see curve 2 in Fig. 6). For an ion-penetrable bacterium, mobile ions inside the ion-penetrable layer yield a conductivity of the bacterial cell surface, which increases double layer polarization (see curve 3 in Fig. 6) [29]. During micro-electrophoresis, electro-osmotic fluid flow may exist inside the ion-penetrable layer [36]. Particles that permit electro-osmotic fluid flow inside their ion-penetrable layer are often referred to as 'electrophoretically soft' particles. For electrophoretically soft bacteria, the slip plane is not located outside but inside the ion-penetrable layer, close to the ion-impenetrable core of the bacterium. The ease with which fluid can flow through the ion-penetrable layer is characterized by the electrophoretic softness λ^{-1} [54] with

$$\lambda = \left(\frac{\gamma}{\eta}\right)^{1/2} \tag{17}$$

with γ the coefficient of friction exerted on liquid flowing through the ion-penetrable layer. The effect of an electrophoretic softness of 2 nm on bacterial electrophoretic mobility [61] is shown in Fig. 6 as well (curve 4). Regardless of ionic strength, electrophoretic softness causes bacteria to have a more negative electrophoretic mobility, as illustrated in Fig. 7. The figure also compares the electric potential and the electro-osmotic fluid flow for an ion-impenetrable bacterium and an electrophoretically hard and soft ion-penetrable bacterium with the same surface potential. The slip plane of

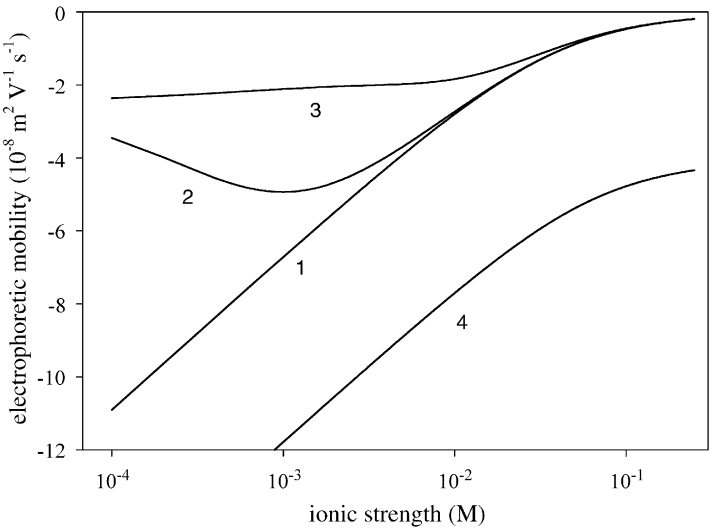

Fig. 6. Electrophoretic mobility of a bacterium covered with an ion-penetrable layer as a function of ionic strength in a 1-1 electrolyte. The bacterial radius (including the ion-penetrable layer) is 0.5 μm and the ion-penetrable layer has a thickness of 50 nm and a fixed charge density of 10×10^6 C/m^3. Curve 1: mobility according to the Helmholtz–Von Smoluchowski equation; curve 2: accounting for double layer polarization [29]; curve 3: accounting for surface conductivity (assuming that the specific conductivity inside the ion-penetrable layer is 40% of the specific conductivity inside the solution) [79]; curve 4: accounting for electrophoretic softness (softness λ^{-1} of 2 nm). All curves are obtained by solving the non-linear Poisson–Boltzmann equation [61].

the ion-impenetrable cell surface is located close to the surface. Similarly, the slip plane of the ion-penetrable, hard cell surface is also located adjacent to the ion-penetrable layer. For the ion-penetrable, soft cell surface, however, the slip plane is located inside the ion-penetrable layer close to the ion-impenetrable core and consequently these cells attain a much higher electrophoretic velocity u_E.

It is not ubiquitously accepted [29] that electrophoretic fluid flow is possible through soft ion-penetrable cell surface layers. Cohen Stuart et al. [62] showed both experimentally and theoretically that fluid flow in-between polymer coated parallel plates in response to an applied pressure difference only penetrates through the outer polymer layers. It can be calculated that in their set-up fluid flow only penetrates the outer 2 nm of a 50 nm thick, ion-penetrable polymer coating with a coefficient of friction γ that would correspond with an electrophoretic softness of 2 nm. Still, by comparison of curves 4 and 1 in Fig. 6, it can be seen that a 50 nm thick layer with a 2 nm electrophoretic softness will have a markedly greater electrophoretic mobility than a hard layer due to a non-negligible electro-osmotic fluid flow in the ion-penetrable layer. Therefore, the nearly complete absence of fluid flow through polymer coatings as measured by Cohen Stuart et al. [62] does not rule out the possibility of electro-osmotic fluid flow through polymer layers present on bacteria. The coefficient of friction that leads to an electrophoretic softness of 2 nm corresponds with a polymer volume density of 20% [62]. This is in the same range as estimates of the volume density of peptidoglycan in the cell wall of Gram-positive bacteria, further supporting the possibility of electro-osmotic flow through the bacterial surface.

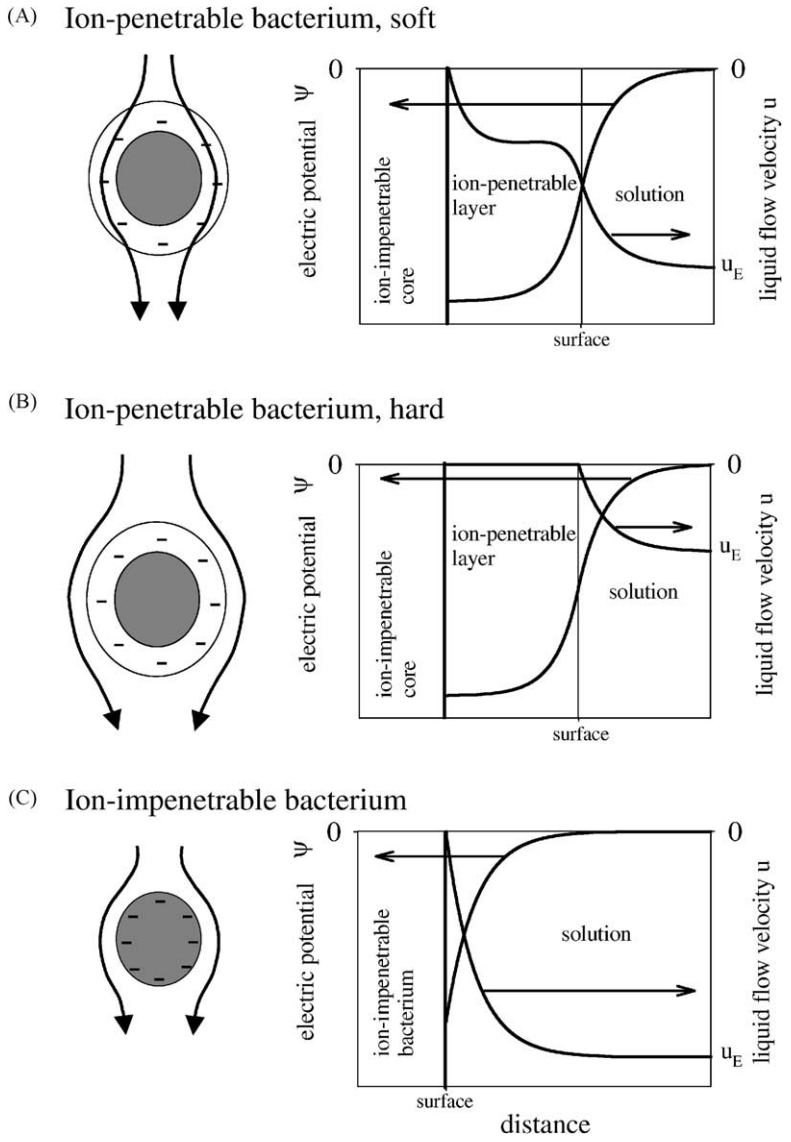

Fig. 7. Schematic presentation of an ion-penetrable, electrophoretically soft and hard bacterium and of an ion-impenetrable cell surface. The distribution of electro-osmotic fluid flow and the electric potential are indicated as a function of distance from the cell surface. Note that for the ion-penetrable bacteria, charge is distributed uniformly over the surface layer, while for the ion-impenetrable bacterium charge is located at the surface. The slip plane is assumed to coincide with the ion-impenetrable surface. Reprinted from Poortinga et al. [32].

The electrophoretic mobility of electrophoretically soft bacteria depends on the charge distribution inside the ion-penetrable layer [61]

$$\mu = \frac{\varepsilon}{\eta}\left[\overline{\psi(x)} + \frac{1}{\lambda^2}\overline{\frac{\rho_{\mathrm{fix}}(x)}{\varepsilon}}\right], \tag{18}$$

where

$$\overline{f(x)} \equiv \lambda \int_0^{d_w} f(x) \exp(\lambda(x - d_w))\, dx \tag{19}$$

with $f(x)$ being either $\psi(x)$ or $\rho_{fix}(x)$. Eqs. (18) and (19) assume a uniform softness λ^{-1} and a thickness of the ion-penetrable layer d_w such that $d_w\lambda \geq 1$. Eq. (19) implies that electrophoresis probes the electric potential and fixed charge density inside the ion-penetrable layer to a depth of several times λ^{-1}.

Soft particle analyses of bacterial cell surfaces have always assumed a uniform charge density through the ion-penetrable layer, yielding an analytical expression for the bacterial electrophoretic mobility at low surface potential [54]

$$\mu = \frac{\rho_{fix}}{\eta\lambda^2}\left[1 + \left(\frac{\lambda}{\kappa}\right)^2 \frac{1 + \lambda/2\kappa}{1 + \lambda/\kappa}\right]. \tag{20}$$

The above equation allows derivation of the bacterial electrophoretic softness and fixed charge density by fitting this equation to measurements of the bacterial electrophoretic mobility as a function of ionic strength, provided that the softness and fixed charge density are constant over the range of ionic strengths employed. Practically, this last condition makes that electrophoretic mobilities measured at ionic strengths below about 5 mM need to be excluded from the fit procedure.

2.4. Experimental data

2.4.1. Electrophoretic mobility and surface charge of bacterial cells

Bacterial electrophoretic mobilities are often measured as a function of pH at constant ionic strength. Fig. 8 shows the pH dependence of the zeta potential calculated from the electrophoretic mobility using the Helmholtz–Von Smoluchowski equation for four selected strains [41] in 10 mM potassium phosphate solutions. The pH dependence of the bacterial zeta potentials is characteristic for a given isolate, but generally is not characteristic at the strain or species level, as isolates with widely different surfaces may exist for a given strain [41]. The pH at which the electrophoretic mobility is zero is referred to as the isoelectric point (IEP). In the absence of specific adsorption, the IEP is determined by the balance between anionic and cationic acid/base groups at the cell surface. IEPs of bacteria have been used to obtain insight in the molecular composition of their surfaces. Rijnaarts et al. [46] distinguished bacteria predominantly covered by anionic polysaccharides with an IEP $\leq$ 2.8, based on the dissociation constants of the constituting molecular groups (see Table 2). Peptidoglycan covered bacterial cell surfaces have an IEP between pH 3.0 and 4.0, while proteinaceous cell surfaces have an IEP exceeding pH 4.0. This classification based on IEPs is supported by observations that tufts of proteinaceous fibrils increase the IEP of a *Streptococcus sanguis* CR311 strain from below pH 2 for a bald variant, to pH 2.8 for the tufted one [41].

More detailed, quantitative information on bacterial cell surface compositions can be derived from proton titration, or from fitting the pH dependence of bacterial charge densities as derived from bacterial zeta potentials using Eq. (8) to the ionizable surface group model [47]. Assuming a negligible electric potential (i.e. a negligible contribution from electrostatic interactions to the Gibbs energy of association or dissociation of molecular groups at the bacterial surface), charge densities can be inserted in Eq. (1) to obtain values for the densities and pK_a's of the surface groups, as given in Table 3.

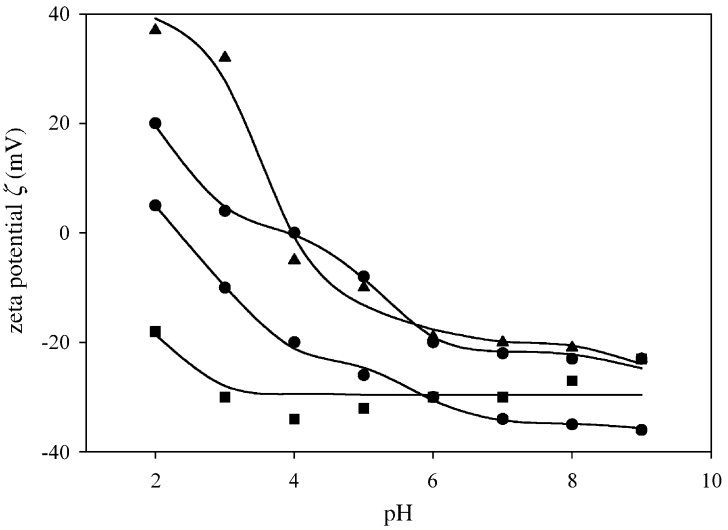

Fig. 8. Zeta potentials calculated from electrophoretic mobilities using the Helmholtz–Von Smoluchowski equation as a function of pH measured in 10 mM phosphate buffer for four different bacterial strains. Lines denote fits to an ionizable surface group model such as Eq. (1), but assuming the bacterial cell surface to contain one amino group and two different kinds of anionic groups (instead of in Eq. (1), where only one anionic group is assumed). Experimental data taken from Busscher et al. [41].

The anionic groups in Table 3 have pK_a values of about 2.5, indicating the presence of either polysaccharide, teichoic acids and/or phospholipids, and pK_a values of about 5, implying the presence of proteins and/or peptidoglycan at the bacterial surface. Note that the surface of *S. epidermidis* HBH 171 appears to lack proteins. In line with this, XPS analyses show that the amount of nitrogen present at the cell surface of this strain is small compared to the amount of oxygen and phosphate [63]. In an alternative approach, Boonaert and Rouxhet [64] calculated the densities of the different ionizable groups present at the cell surface of *Lactobacillus helveticus* from surface compositions obtained by XPS. These densities were used to derive the surface charge density of the strain as a function of pH according to Eq. (1), either assuming the electric potential at the location of the ionizable groups to be zero or equal to 10 times the bacteria zeta potential [65]. The first assumption led to a pH dependence of the bacterial zeta potentials similar to experimental ones.

Table 3
Parameters obtained from fitting the bacterial surface charge (as derived from the bacterial zeta potential using Eq. (8)) as a function of pH as shown in Fig. 8 for four bacterial strains to an ionizable surface group model assuming the bacterial surface to contain N_1 amino groups per square meter with a pK_{a1} of 9.5 and two different anionic groups with densities N_2 and N_3 and pK_a values pK_{a2} and pK_{a3}, respectively

Bacterium	N_1 ($\times 10^{16}$ m^{-2})	pK_{a2}	N_2 ($\times 10^{16}$ m^{-2})	pK_{a3}	N_3 ($\times 10^{16}$ m^{-2})
E. coli 2239	1.9	2.9	6.3	5.7	2.5
S. epidermidis HBH 171	0	1.8	6.2	–	0
S. mitis 398	8.5	3.5	11.5	5.8	1.3
L. acidophilus ATCC 9224	6.4	2.2	6.3	5.2	4.7

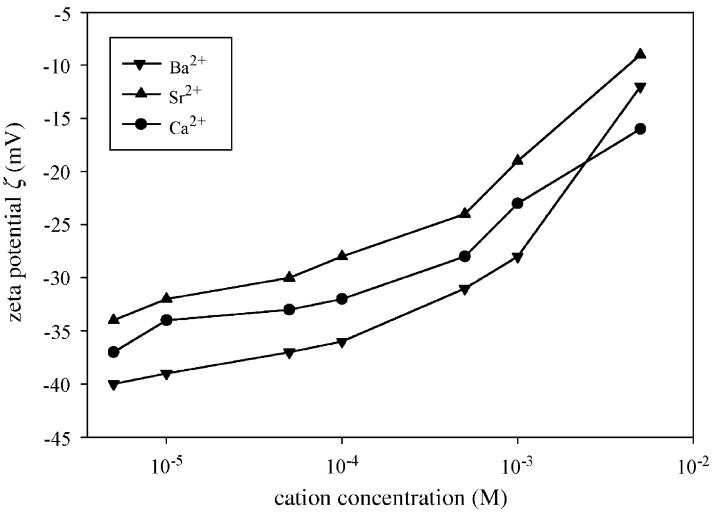

Fig. 9. Zeta potentials of *B. subtilis* ATCC 6051 as calculated from the electrophoretic mobility using the Helmholtz–Von Smoluchowski equation as a function of cation (Ba^{2+}, Sr^{2+}, Ca^{2+}) concentration measured at a pH of around 8 with the total ionic strength kept at 15 mM using NaCl. Data taken from Chang and Hsieh [49].

The ionizable surface group model cannot completely explain the pH dependence of bacterial zeta potentials. For example, often an increase in bacterial zeta potentials at elevated pH is observed, as for *S. epidermidis* HBH 171 in Fig. 8 that cannot be explained by progressive dissociation of negatively charged groups. Since streptococcal and staphylococcal diffusion coefficients have been shown to decrease with increasing pH [66], amongst other things due to the extension of fibrils, it is likely that ion-penetrable layers swell with increasing pH and thus reduce the bacterial charge density and electrophoretic mobility. AFM data have also indicated extension of fibrils upon lowering the ionic strength of streptococcal suspensions to below 0.1 M due to increased electrostatic repulsion between the fibrils [67]. Plette et al. [68] described swelling of *Rhodococcus erythropolis* A177 cell walls below 0.1 M and above pH 5 and found that the volume of the peptidoglycan layer doubles when the ionic strength decreases from 0.1 to 0.01 M.

The bacterial cell surface also acquires charge by specific adsorption of, in particular, multivalent cations [49,50,69,70] like for instance Ca^{2+} from saliva [51]. Specific adsorption of multivalent cations to bacterial surfaces depends on their ability to form chemical bonds with negatively charged surface groups [68,71], like carboxyl and phosphate groups [71]. Fig. 9 shows the zeta potentials of *Bacillus subtilis* ATCC 6051 as a function of cation concentration [49]. Assuming that bacterial zeta potentials equal the diffuse double layer potential, it was demonstrated that specific cation adsorption obeys a modified Langmuir isotherm (Eq. (2)), with adsorption energies $\Delta_{ads}G$ ranging from 13.4 kT for Sr^{2+} to 10.9 kT for Ba^{2+}, comparable to the energy of proton binding to carboxyl groups in proteins. Even if not specifically interacting with the bacterial surface, multivalent cations greatly influence surface charge properties of bacteria as they are highly concentrated in the ion-penetrable layer (see Eq. (6)). Wasserman and Felmy [72], for example calculated that the presence of only 10^{-6} M trivalent cations in 1 mM 1-1 electrolyte is able to increase the Donnan potential from −110 to −85 mV.

It should be noted that as bacterial surfaces are inherently heterogeneous, the bacterial electrophoretic mobility only yields an average value of the bacterial surface charge while major local differences can be

Table 4
Fixed charge densities ρ_{fix} and electrophoretic softness λ^{-1} of different bacterial strains collected from literature for different pH, together with information on the bacterial surface structure (if presented)

Bacterium	ρ_{fix} ($\times 10^6$ C/m^3)	λ^{-1} (nm)	pH	Remarks	Reference
Streptococci					
S. salivarius HB	−1.2	1.5	5	Fibrillated	[31]
S. salivarius HB-C12	−1.4	0.8	5	Non-fibrillated	[31]
S. oralis J22	−2.1	1.6	7	–	[97]
Staphylococci					
S. aureus	−2.2	1.5	5	–	[36]
S. aureus	−2.9	2.0	9	–	[36]
*S. epidermidis*3399	−2.0	3.2	6	Encapsulated	[74]
S. epidermidis ATCC 35983	−2.7	1.9	6	Slime producing, grown in broth	[74]
S. epidermidis ATCC 35983	−1.1	4.2	6	Slime producing, grown on agar	[74]
Miscellaneous					
E. coli	−7.2	0.5	3	–	[36]
E. coli	−14.4	0.7	9	–	[36]
Pseudomonas Syringae NIAES 1309	−0.2	3.8		Sugar-rich surface	[75]
V. alginolyticus YM 4	−0.4	6.4	7	Flagellar	[55]

expected on a molecular scale. Using atomic force microscopy, Fang et al. [73], for instance, found that the attractive force between the AFM tip and the surface of sulfate-reducing bacteria varied from 3.9 to 4.3 nN along the bacterial surface.

2.4.2. *Ion-penetrability and electrophoretic softness of bacterial cell surfaces*

Until now, relatively few studies have employed a soft particle model (for example Eq. (20)) to describe bacterial cell surfaces. Table 4 summarizes fixed charge densities and electrophoretic softness values as found in the literature for several bacterial strains. Fixed charge densities and electrophoretic softnesses differ widely for various strains depending on the bacterial surface structure and culture conditions. The soft particle model can identify several features of bacteria that remain undiscovered when using the Helmholtz–Von Smoluchowski equation. For example, a soft particle analysis shows that the surface of *Pseudomonas syringae* NIAES 1309 is covered with (uncharged) sugar molecules having a low fixed charge density despite of a considerable electrophoretic mobility (see Table 4). Also, the fibrillated *S. salivarius* HB has a smaller fixed charge density than its non-fibrillated mutant HB-C12 as revealed by the soft particle model (see Table 4), whereas applying the Helmholtz–Von Smoluchowski equation yields a greater surface charge for the fibrillated strain because of its greater electrophoretic mobility [31].

Fixed charge densities in Table 4 are in the order of 3×10^6 C/m^3, which is threefold lower than obtained from titration experiments [29,76]. Most probably, the bacterial ion-penetrable layer is less dense and consequently carries less fixed charges at its outer surface than deeper inside the ion-penetrable layer. As, according to Eq. (19), electrophoresis mainly probes the fixed charge density of the outer part of the ion-penetrable layer, whereas titration measures the total fixed charge density inside the ion-penetrable layer, particulate micro-electrophoresis yields a lower fixed charge density

than titration. Because bacterial adhesion to surfaces is an interaction between outer surfaces, charge densities obtained from electrophoresis are likely more relevant to calculate bacterial electric double layer interactions than those obtained from titration experiments.

The electrophoretic softness and fixed charge density obtained from soft particle analyses have been shown to correlate in a meaningful way with bacterial cell surface properties obtained from other measurements, indicating the validity of the soft particle model. For example, *S. salivarius* HB-C12 exhibits a smaller softness and a greater fixed charge density than *S. salivarius* HB (see Table 4), in accordance with the observation of fibrils on the latter. Also, electrophoretic softness of the ion-penetrable layer has been found to positively correlate with the mechanical softness of several streptococcal strains as measured with AFM [67].

2.5. Concluding remarks

The bacterial cell surface is charged by dissociation and association of ionizable surface groups and specific adsorption, especially of multivalent cations. Structural cell surface features present themselves as an ion-penetrable layer on the bacterial cell wall, yielding a high surface conductivity and permitting electro-osmotic flow through the ion-penetrable layer ('electrophoretic softness'). Bacterial cell surface charge strongly changes in response to environmental factors, therewith contributing to the dynamic nature of bacterial cell surfaces.

3. Electric double layer interactions in bacterial adhesion: theoretical

Electric double layer interactions in colloidal particle adhesion according to the DLVO theory have recently been reviewed by Adamczyk and Warszýnski [52] and the present review will be confined to the deviations from classical electric double layer interactions as described in the DLVO theory due to the characteristic properties of bacterial cell surfaces.

3.1. Dynamics of electric double layer interactions in bacterial adhesion

Both the fixed and the diffuse charge densities at bacterial cell surfaces depend on the local electric potential (see Eqs. (1) and (6)). For an isolated bacterium, the electric potential distribution at its surface is determined solely by its own fixed charge (and the diffuse counter charge attracted by it), but upon interaction with another surface, fixed charges present at that surface also contribute to the electric potential distribution at the bacterial cell surface. Consequently, the electric potential distribution and, in response, the fixed and diffuse charge densities at the bacterial cell surface change during electric double layer interaction with another surface.

The adjustment of charge densities during electric double layer interactions is a kinetic process involving several simultaneously occurring steps, each with a characteristic time constant. First, the time required for a bacterium to diffuse across an electric double layer with thickness $1/\kappa$ can be calculated from [40,77]

$$\tau_{\text{bacterium}} = \frac{1}{2D_{\text{b}}\kappa^2} \tag{21}$$

in which D_b is the bacterial diffusion constant. According to Eq. (21), a bacterium with a radius of 500 nm and a diffusion constant of 10^{-12} m^2 s^{-1}, needs approximately 10^{-5} s to cross a 10 nm thick electric double layer. Similarly, the diffusion time of ions with diffusion constant D_i during interaction of a particle with radius a with a flat surface can be estimated from [78]

$$\tau_{ion} = \frac{a}{2D_i\kappa}. \tag{22}$$

For bacteria, diffuse double layer charges are not only present inside the solution, but also inside the ion-penetrable layer. van der Wal et al. [79] found that the diffusion constant of ions inside the peptidoglycan layer is about 40% of that inside solution. For a diffusion constant of 5×10^{-10} m^2 s^{-1} (40% of the ion diffusion constant in solution) and a 10 nm thick double layer, redistribution of diffuse double layer charges takes about 10^{-6} s according to Eq. (22). Note that this is substantially smaller than the time required for a bacterium to cross the electric double layer, indicating that diffuse double layer ions remain in thermodynamic equilibrium during bacterial–substratum interaction, i.e. the distribution of diffuse double layer ions obeys the Poisson–Boltzmann equation. The time required for the fixed charge density to adjust during interaction is given by [77]

$$\tau_{charge} = \frac{RTC}{eN_A i_0} \tag{23}$$

with R the gas constant and C the interfacial capacitance. The rate at which charge is exchanged between groups at the bacterial surface and the solution, i_0, can differ drastically between one system to another ranging between 10^{-10} and 1 A/cm^2 [78]. Typically, according to Eq. (23) the characteristic time of an adjustment in fixed charge density is between 2500 s and 0.25 μs. If adjustment of the fixed charge density takes longer than it takes a bacterium to cross the diffuse double layer of a substratum surface (approximately 10^{-5} s), the fixed charge density remains constant during interaction. Experimental studies have shown that the strength of bacterial adhesive bonds increases as a function of time, with a characteristic time constant of around 10 s [80]. This may indicate that adjustment of fixed charges at bacterial cell surfaces indeed takes longer than the time needed for a bacterium to cross the electric double layer of a substratum to adhere to it.

When, on the other hand, the adjustment of fixed charges at the bacterial cell surface proceeds faster than the rate at which a bacterium crosses the electric double layer, the fixed charge density is always regulated to maintain equilibrium during interaction [81]. There are two extreme cases of charge-regulation: either the fixed charge density remains constant or the fixed charge density adjusts in such a way that the electric potential inside the ion-penetrable layer remains constant during electric double layer interaction. Hitherto, a constant potential distribution inside the ion-penetrable layer has been assumed in most studies on electric double layer interactions in bacterial adhesion [2–5]. Since the electric potential inside the ion-penetrable layer is assumed constant, it is irrelevant whether or not diffuse interfacial charges can move through the ion-penetrable surface layer [82], i.e. ion-penetrability of the bacterial surface becomes irrelevant. At low electric potential, when the Poisson–Boltzmann equation may be linearized, the constant potential approximation yields for the energy of electric double layer interaction between a spherical bacterium and a flat substratum [83]

$$V_{el}(h) = a\varepsilon\pi(\psi_{01}^2 + \psi_{02}^2)\left(\frac{2\psi_{01}\psi_{02}}{\psi_{01}^2 + \psi_{02}^2}\ln\left[\frac{1+\exp(-\kappa h)}{1-\exp(-\kappa h)}\right] + \ln(1-\exp(-2\kappa h))\right) \tag{24}$$

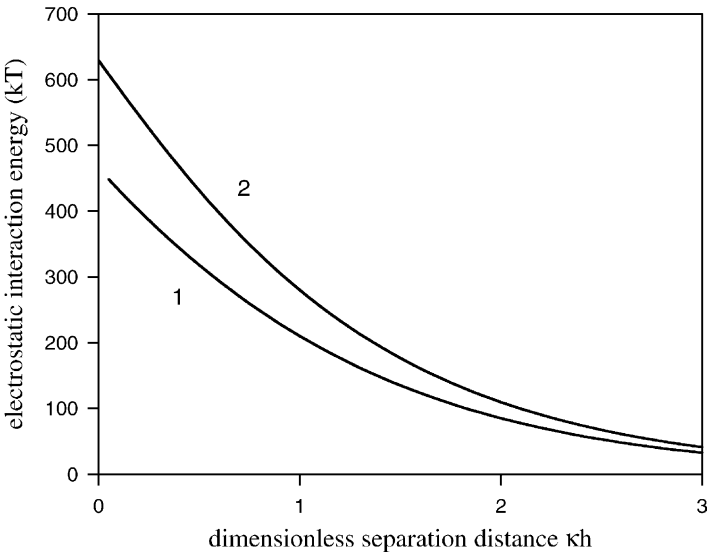

Fig. 10. Electric double layer interaction energy between an ion-penetrable sphere and a flat ion-impenetrable plate, both with a surface potential of −25 mV, as a function of the dimensionless surface to surface separation distance κh. Curve 1: assuming constant surface potentials during interaction (Eq. (24)); curve 2: assuming constant fixed charge densities during interaction (Eq. (25)).

with ψ_{01} and ψ_{02} the surface potentials of the interacting surfaces and h the surface to surface separation distance.

Alternatively, assuming a constant fixed charge density during interaction, the electric double layer interaction energy of a spherical ion-penetrable bacterium interacting with an ion-impenetrable flat substratum is given by [84]

$$V_{\mathrm{el}}(h) = 4\pi\varepsilon a\left[\psi_{01}\psi_{02}\exp(-\kappa h) - \frac{1}{4}\psi_{02}^2\frac{a}{a+h}\exp(-2\kappa h)\right] \tag{25}$$

with ψ_{02} the bacterial surface potential, which is related to the fixed charge density through

$$\psi_{02} = \frac{\rho_{\mathrm{fix}}}{2\varepsilon\kappa^2}. \tag{26}$$

Fig. 10 compares the constant potential and constant fixed charge approaches. Clearly, repulsive electric double layer interaction energies calculated at constant potential are smaller than at constant fixed charge. During interaction, the diffuse double layers present at the interacting surfaces are compressed, leading to a decrease in interfacial capacitance. Hence, in order to maintain a constant fixed charge density, the electric potential needs to increase, which leads to a larger electric double layer repulsion compared with the constant potential approach. In order to determine whether the constant potential or constant fixed charge approach describes the charge-regulation behavior of bacteria during interactions best, the fixed charge density of the bacterial cell surface has to be known as a function of the electric potential. At low electric potential the relation between fixed charge density and electric potential can be approximated by [85,86]

$$\rho_{\mathrm{fix}}(\psi) = \rho_0 - K\psi \tag{27}$$

with

$$\rho_0 \equiv \rho_{\mathrm{fix}}(\psi = 0), \tag{28}$$

$$K \equiv -\left.\frac{\partial \rho_{\mathrm{fix}}(\psi)}{\partial \psi}\right|_{\psi=0} \tag{29}$$

in which K is the charge-regulation capacitance. K is always positive and its magnitude reflects the tendency of ionizable groups to oppose changes in the electric potential by shifting their ionization equilibria. Consequently, $K = 0$ and ∞ correspond with constant fixed charge and constant potential, respectively.

The charge-regulation capacitance can be calculated from the ionizable surface group model (Eqs. (1) and (29)) provided that the densities of the different ionizable surface groups and their dissociation constants are known, as determined by van der Wal et al. [30] for several Gram-positive strains using proton titration. The charge-regulation capacitance calculated (see Fig. 11) shows maxima at the pK_a's of the different ionizable groups present and is found not to exceed 3×10^7 F/m^3. Since Gram-positive bacterial cell surfaces usually contain little phosphate [63], it can be inferred from Fig. 11 that their fixed charge density will remain constant during interaction with surfaces at pH values between 6 and 10. Fig. 12 presents the electric double layer interaction energy as a function of ionic strength, calculated for two separation distances between two ion-penetrable surfaces using the low potential approximation, while accounting for charge-regulation. Deviations from constant fixed charge do not influence the calculated electric double layer interaction energies for ionic strengths above 10 mM, indicating that the constant fixed charge approach is a valid approximation in this range of ionic strengths. Note that for each separation distance, an increase in the charge-regulation capacitance leads to a smaller electric double layer interaction energy.

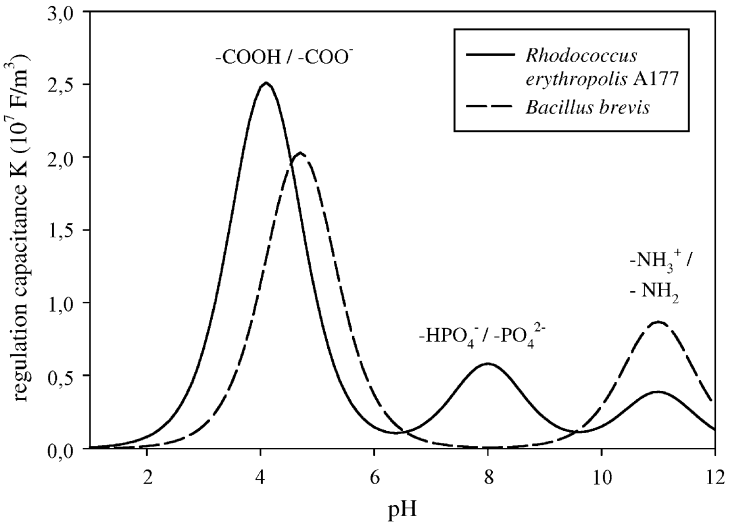

Fig. 11. Charge-regulation capacitance as defined by Eq. (29) as a function of pH for two bacterial strains calculated using the ionizable surface group model with densities of ionizable groups and their K_a values taken from titration data of van der Wal et al. [30]. The net fixed charge density has been rescaled to give 3×10^6 C/m^3 at pH 7. The ionizable group that contributes most to the charge-regulation capacitance in a given region of pH is indicated.

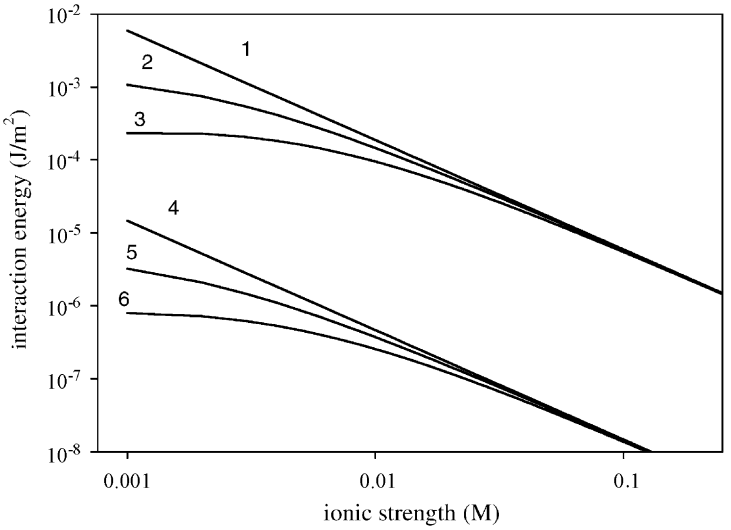

Fig. 12. Electric double layer interaction energy for the interaction of two similar charge-regulating ion-penetrable plates calculated assuming low electric potential [84] and a fixed charge density of 3×10^6 C/m^3 as a function of the ionic strength of a 1-1 electrolyte solution for different values of the charge-regulation capacitance K and of the surface to surface separation distance h. Curve 1: $h = 0$, $K = 0$; curve 2: $h = 0$, $K = 10^7$ F/m^3; curve 3: $h = 0$, $K = 3 \times 10^7$ F/m^3; curve 4: $h = 3\kappa^{-1}$, $K = 0$; curve 5: $h = 3\kappa^{-1}$, $K = 10^7$ F/m^3; curve 6: $h = 3\kappa^{-1}$, $K = 3 \times 10^7$ F/m^3.

The charge-regulation behavior of ion-impenetrable particles and its dependence on the Stern layer capacitance was studied by Behrens and Borkovec [87], who found that when the interfacial capacitance of particles is dominated by the Stern layer capacitance the constant potential description is preferred. For latex particles, for which the Stern layer hardly contributed to the interfacial capacitance, it was found that the diffuse double layer capacitance exceeded the regulation capacitance over a wide range of pH and ionic strengths and by consequence the particles exhibit constant charge behavior. This will be even more true for bacteria, that due to their ion-penetrability, lack a Stern layer and have a high diffuse double layer capacitance (given by ρ_{fix}/ψ_0 as derived from Eq. (26)).

3.2. *Effect of heterogeneities on electric double layer interactions in bacterial adhesion*

Bacterial surfaces are chemically and structurally heterogeneous, but in almost all cases detailed knowledge of bacterial cell surface properties at the nanometer level is lacking. Elimelech and O'Melia [88] proposed to theoretically account for structural surface heterogeneities by composing a surface, covered by small semi-spheres with a 20 nm radius. This led to a decrease in the interaction energy barrier experienced by a 0.4 μm sphere from 23 to 11 kT in 0.01 M 1-1 electrolyte. The reason for this is that the sphere partially interacts with the semi-spheres which, due to their small dimensions, cause smaller repulsion. Elimelech and O'Melia [88] also accounted for heterogeneous surface charge distributions on interacting surfaces by assuming the charge density to follow a Gaussian distribution around its average value and by calculating a weighted average of the theoretical particle deposition rates at all combinations of surface charges. This led to a better correspondence between theoretical and experimental results and indicated that surface charge heterogeneity decreases the influence of electric

double layer repulsion on adhesion. This method does not account for the fact that during interaction a particle with a heterogeneously charged surface may reorient to contact an electrostatically repelling substratum surface with its least charged site, to further decrease electric double layer repulsion [89].

3.3. Concluding remarks

Electric double layer interactions during bacterial adhesion lead to redistribution of charges. It is argued on theoretical grounds that adjustment of fixed charges in the bacterial cell surface proceeds slower than the rate at which bacteria approach a substratum and consequently the fixed charge density can be assumed to be constant during interaction. Even when fixed charges in the bacterial cell surface adjust quickly during interaction, a constant fixed charge approach performs well, except for low ionic strengths. Theoretical analyses show that a heterogeneous distribution of surface charges reduces electric double layer repulsion during bacterial adhesion.

4. Electric double layer interactions in bacterial adhesion: experimental

4.1. Comparison of experimental and theoretical results

Electric double layer interactions in bacterial adhesion to surfaces have hitherto mostly been investigated indirectly, by studying the adhesion or desorption of adhering bacteria in media of different ionic strengths [10,90–92] or pH [75,93] or to substrata with different surface potentials [9,94,95]. Recently, electric double layer interactions in bacterial adhesion have been studied more directly using electrode surfaces as a substratum, which allows variation of the substratum potential in situ [96,97]. In line with theoretical expectations, van der Mei et al. [94] found a strong, nearly linear, decrease in deposition efficiency of six staphylococcal strains depositing on two differently charged substrata as a function of the calculated electric double layer repulsion. Similarly, Fig. 13 gives an example of the deposition efficiency of a negatively charged bacterium depositing to a negatively charged substratum as a function of ionic strength, showing a decreased deposition efficiency with decreasing ionic strength due to electric double layer repulsion.

Assuming that the experimental data in Fig. 13 represent primary minimum adhesion, because experiments were conducted under high shear [88], theoretical deposition efficiencies α indicated in Fig. 13 were calculated using

$$\alpha = \exp\left(-\frac{V_{\max}}{kT}\right) \tag{30}$$

with $V_{\max}$ being the energy barrier for deposition in the primary interaction minimum. Two approaches have been used to account for electric double layer repulsion in calculating the energy barrier: (1) by analyzing the bacterial electrophoretic mobility using the Helmholtz–Von Smoluchowski equation, i.e. neglecting electrophoretic softness, assuming constant surface potentials (i.e., using Eq. (24)) equal to the zeta potentials and (2) by accounting for electrophoretic softness using Eq. (20) and assuming constant fixed charge densities (Eq. (25)). By comparison, higher deposition efficiencies are calculated when the bacterium is considered electrophoretically soft and maintaining a constant fixed charge density than when it is considered electrophoretically hard under constant surface potential conditions.

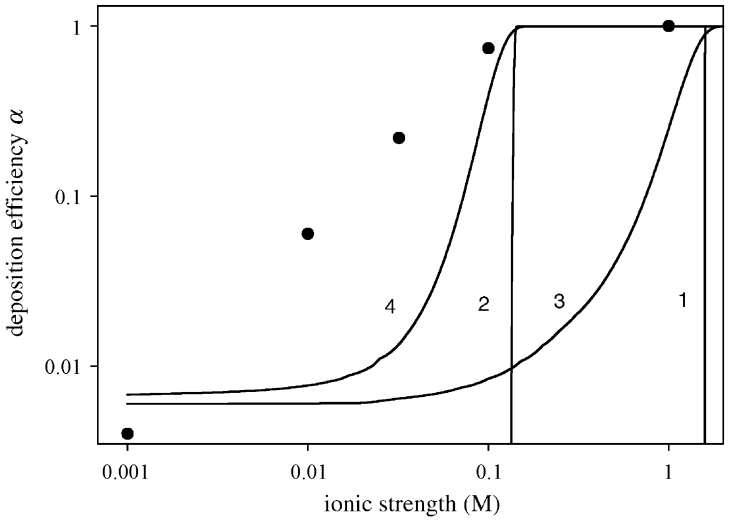

Fig. 13. Deposition efficiency of *Corynebacterium* sp. DSM 6688 depositing to Teflon (points) compared with DLVO calculations assuming a low electric potential (lines). Experimental data taken from Rijnaarts et al. [98]. Curve 1: electrophoretically hard bacterium, homogeneous surfaces maintaining constant potential; curve 2: electrophoretically soft bacterium, homogeneous surfaces maintaining constant fixed charge; curve 3: same as curve 1, but with a heterogeneously charged substratum; curve 4: same as curve 2, but with a heterogeneously charged substratum.

In order to show the effect of surface charge heterogeneity on the deposition efficiency, the substratum surface potential can be assumed to follow a Gaussian distribution with a standard deviation of 40% of its average value, to obtain a weighed average of the deposition efficiencies at different substratum potentials [88]. As can be seen in Fig. 13 for deposition of *Corynebacterium* sp. DSM 6688, this yields better correspondence between theoretical and experimental results than obtained assuming homogeneous charge distribution.

We have shown that the soft particle model can reveal several features of bacterial surface charge that remain undiscovered when using the Helmholtz–Von Smoluchowski equation. Therefore, use of the soft particle model may explain hitherto obscure differences in adhesive behavior of bacteria (see [18,24,26] in Table 1). Fig. 14 exemplifies this by comparing the deposition of a fibrillated and a non-fibrillated *Streptococcus salivarius* mutant to glass. Lines denote theoretical deposition efficiencies as obtained from an analysis of bacterial mass transport [42] (these may exceed one due to sedimentation of bacteria). Fig. 14 also includes a schematic picture of bacteria modeled as ion-penetrable. The presence of fibrils leads to a lower fixed charge density in the outer layers of the bacterium, as detected using the soft particle model (see Table 4), and consequently leads to enhanced adhesion, both theoretically and experimentally. By contrast, an analysis based on the Helmholtz–Von Smoluchowski equation predicts slightly higher deposition efficiencies for the non-fibrillated strain [18].

Several other discrepancies between theory and experiments on bacterial adhesion, listed in Table 1, can be explained by accounting for cell surface softness and ion-penetrability. Many authors (see Table 1) [16,99] have overestimated the role of electric double layer repulsion in bacterial adhesion, because they did not account for electrophoretic softness and surface heterogeneity of bacteria. Decreasing deposition efficiencies with increasing ionic strength above 0.1 M (see also Table 1) can be attributed to a decrease in the thickness of the ion-penetrable layer, which increases the fixed charge

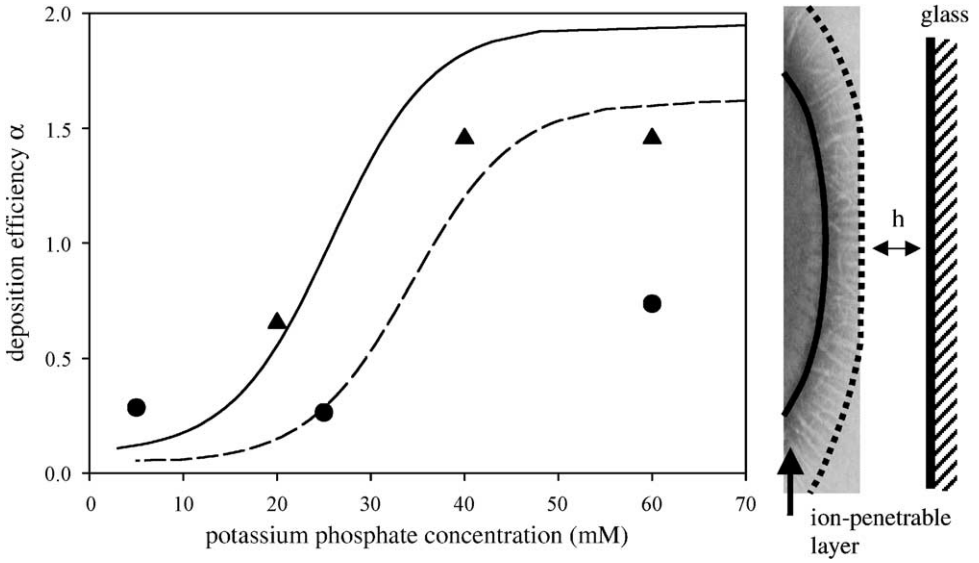

Fig. 14. Deposition efficiency as a function of potassium phosphate concentration for the fibrillated *S. salivarius* HB (▲, drawn line) and the non-fibrillated *S. salivarius* HB-C12 (●, dashed line) depositing to glass, including schematic picture of the model used. Experimental data from Sjollema et al. [18] and Poortinga et al. [32]. Lines: calculated from an analysis of bacterial mass transport including the influence of bacterium–substratum interactions [42], assuming a heterogeneous substratum [32].

density inside this layer and hence opposes adhesion. Schäfer et al. [22] found a decreasing deposition efficiency for ionic strengths exceeding 1 mM. Likely due to adhesion arising from positively charged domains at the bacterial surface yielding electric double layer attraction with negatively charged substratum surface (as observed by Zita and Hermansson [20] and Cowan et al. [100], see Table 1).

4.2. Other physico-chemical interactions in bacterial adhesion

As mentioned in Section 1, forces other than classical DLVO interaction forces play a role in bacterial adhesion. Although in this review proposals have been made to improve our understanding of electric double layer interactions in bacterial adhesion, other interactions should be taken into account as well. McEldowney and Fletcher [23] and van Loosdrecht et al. [101] emphasized the importance of hydration forces to explain that the number of bacteria adhering to hydrophilic substrata decreased with increasing electric double layer repulsion while electric double layer repulsion had a negligible influence on adhesion to hydrophobic substrata. Hydration forces operative between hydrophilic surfaces are repulsive and decay exponentially with an estimated decay length of 0.6 nm, whereas hydration forces operative between hydrophobic surfaces are attractive (hydrophobic attraction) and have a proposed decay length of 2 nm [102]. At sufficiently high ionic strength, when electric double layer interactions are relatively short range, hydrophobic attraction may exceed electric double layer repulsion.

Camesano and Logan [27] observed a repulsive force working between a bacterial surface and an AFM tip that extended over more than 100 nm, which is a fivefold longer distance than electric double

layer interactions under the experimental conditions. This force is assigned to steric interactions. Steric interactions result from the presence of surface polymers and are repulsive when long chain bacterial surface polymers, as in an ion-penetrable layer, do not adhere to a substratum, due to, for example insufficient Lifshitz–van der Waals attraction [103–105]. This gives rise to a repulsive force, as the polymers resist compression and therewith prevent the core of the bacterium from reaching the substratum. This is referred to as steric repulsion or steric hindrance. In case of polyelectrolytes, steric interactions are directly related to electric double layer interactions, since the electric potential influences the conformation of the adsorbed polyelectrolyte molecules.

Steric interactions may also be attractive. Due to their small dimensions, charged surface polymers hardly experience any electrostatic barrier towards their adhesion and therewith the presence of these polymers essentially decrease electric double layer repulsion between surfaces. The situation in which surface polymers bridge the gap between two surfaces that repel each other electrostatically is referred to as 'bridging'. Under the condition of constant charge, the presence of ion-penetrable layers at similarly charged surfaces strongly decreases electric double layer repulsion in-between these surfaces [32]. Modeling a layer of charged surface polymers, as may be present on bacteria, as an ion-penetrable layer that maintains a constant charge during interaction with a substratum, therefore may offer a way to incorporate bridging effects of surface polymers.

4.3. Concluding remarks

Electric double layer interactions play an important role in bacterial adhesion to surfaces, as adhesion has been shown to depend on ionic strength and pH of the suspending solution and on the surface potentials of bacteria and substrata. Although the DLVO theory describes interactions between surfaces, it could hitherto not explain many experimental observations because, at least as far as electric double layer interactions are concerned, specific characteristics of bacterial cell surfaces were not properly incorporated. In this review, it is presented how the variety of different bacterial cell surface structures can be accounted for by describing bacteria as ion-penetrable particles with their electrochemical properties derived from electrophoretic mobility measurements using a soft particle model. These advances could be used to resolve previously described discrepancies between experimental data on bacterial adhesion and theoretical predictions based on the DLVO theory. The present review on bacterial electric double layer interactions cannot, however, provide a full, comprehensive theory describing each and every aspect of bacterial adhesion valid for all bacterial strains and species, as bacterial adhesion is a complicated interplay of different interaction forces acting in concert.

References

[1] C.J. Van Oss, Interfacial Forces in Aqueous Media, Marcel Dekker, New York, 1994.
[2] R. Bos, H.C. van der Mei, H.J. Busscher, FEMS Microbiol. Rev. 23 (1999) 179.
[3] M. Hermansson, Colloid. Surf. B 14 (1999) 105.
[4] P.R. Rutter, B. Vincent, in: R.C.W. Berkely, J.M. Lynch, J. Melling, V.P.R. Rutter, B. Vincent (Eds.), Microbial Adhesion to Surfaces, Ellis Horwood, London, 1980.
[5] J. Škvarla, J. Chem. Soc., Faraday Trans. 89 (1993) 2913.
[6] S. Notermans, J.A.M.A. Dormans, G.C. Mead, Biofouling 5 (1991) 21.
[7] J. Visser, T.J.M. Jeurnink, Exp. Heat Fluid Sci. 14 (1997) 407.

[8] G. Harkes, J. Feijen, J. Dankert, Biomaterials 12 (1991) 853.
[9] J. Satou, A. Fukunaga, N. Satou, H. Shintani, K. Okuda, J. Dental Res. 67 (1988) 588.
[10] A.L. Mills, J.S. Herman, G. Hornberger, T.H. DeJesús, Appl. Environ. Microbiol. 60 (1994) 3300.
[11] N. Mozes, F. Marchal, M.P. Hermesse, J.L. van Haecht, L. Reuliaux, A.J. Leonard, P.G. Rouxhet, Biotechnol. Bioeng. 30 (1987) 439.
[12] J.D. Bryers, Biofilms in biotechnology, in: W.G. Characklis, K.C. Marshall (Eds.), Biofilms, Wiley, New York, 1990.
[13] R. Bos, H.J. Busscher, Colloid. Surf. B 14 (1999) 169.
[14] H.J. Busscher, M.N. Bellon-Fontaine, N. Mozes, H.C. van der Mei, J. Sjollema, O. Cerf, P.G. Rouxhet, Biofouling 2 (1990) 55.
[15] B.A. Jucker, H. Harms, A.J.B. Zehnder, J. Bac. 178 (1996) 5472.
[16] H.H.M. Rijnaarts, W. Norde, J. Lyklema, A.J.B. Zehnder, Colloid. Surf. B 14 (1999) 179.
[17] M.C.M. van Loosdrecht, J. Lyklema, W. Norde, A.J.B. Zehnder, Microbiol. Ecol. 17 (1989) 1.
[18] J. Sjollema, H.C. van der Mei, H.M.W. Uyen, H.J. Busscher, J. Adhesion Sci. Technol. 4 (1990) 765.
[19] K.C. Marshall, R. Stout, R. Mitchell, J. Genet. Microbiol. 68 (1971) 337.
[20] A. Zita, M. Hermansson, Appl. Environ. Microbiol. 63 (1997) 1168.
[21] A.S. Gordon, F.J. Millero, Appl. Environ. Microbiol. 47 (1984) 495.
[22] A. Schäfer, H. Harms, A.J.B. Zehnder, Environ. Sci. Technol. 32 (1998) 3704.
[23] S. McEldowney, M. Fletcher, Appl. Environ. Microbiol. 52 (1986) 460.
[24] J. Azeredo, J. Visser, R. Oliveira, Colloid. Surf. B 14 (1999) 141.
[25] S.F. Simoni, H. Harms, T.N.P. Bosma, A.J.B. Zehnder, Environ. Sci. Technol. 32 (1998) 2100.
[26] Y.L. Ong, A. Razatos, G. Georgiou, M.M. Sharma, Langmuir 15 (1999) 2719.
[27] T.A. Camesano, B.E. Logan, Environ. Sci. Technol. 34 (2000) 3354.
[28] I.C. Hancock, in: N. Mozes, P.S. Handley, H.J. Busscher, P.G. Rouxhet (Eds.), Microbial Cell Surface Analysis, VCH, New York, 1991, p. 21.
[29] A. van der Wal, M. Minor, W. Norde, A.J.B. Zehnder, J. Lyklema, Langmuir 13 (1997) 71.
[30] A. van der Wal, W. Norde, A.J.B. Zehnder, J. Lyklema, Colloid. Surf. B 9 (1996) 81.
[31] R. Bos, H.C. van der Mei, H.J. Busscher, Biophys. Chem. 74 (1998) 251.
[32] A.T. Poortinga, R. Bos, H.J. Busscher, Colloid. Surf. B 20 (2001) 105.
[33] J. Yang, R. Bos, G.F. Belder, J. Engel, H.J. Busscher, J. Colloid Interf. Sci. 220 (1999) 410.
[34] P.R. Rutter, in: A.S.G. Curtis, J.D. Pitts (Eds.), Cell Adhesion and Motility, Cambridge University Press, Cambridge, 1980, p. 103.
[35] K.C. Marshall, in: N. Mozes, P.S. Handley, H.J. Busscher, P.G. Rouxhet (Eds.), Microbial Cell Surface Analysis, VCH, New York, 1991, p. 3.
[36] R. Sonohara, N. Muramatsu, H. Ohshima, T. Kondo, Biophys. Chem. 55 (1995) 273.
[37] H. Ohshima, T. Kondo, J. Colloid Interf. Sci. 155 (1993) 499.
[38] S.M. Hammond, P.A. Lambert, A.N. Rycroft, The Bacterial Cell Surface, Croom Helmm, London and Sydney, 1984.
[39] H.C. Tsien, G.D. Shockman, M.L. Higgins, J. Bac. 133 (1978) 372.
[40] J.M. Kleijn, H.P. van Leeuwen, in: A. Baszkin, W. Norde (Eds.), Physical Chemistry of Biological Interfaces, Marcel Dekker, New York.
[41] H.J. Busscher, R. Bos, H.C. van der Mei, P.S. Handley, in: A. Baszkin, W. Norde (Eds.), Physical Chemistry of Biological Interfaces, Marcel Dekker, New York.
[42] J. Sjollema, H.J. Busscher, J. Colloid Interf. Sci. 132 (1989) 382.
[43] D.C. Ellowood, J. Melling, P.R. Rutter, Adhesion of Microorganisms to Surfaces, Academic Press, London, 1979.
[44] E. Dudman, in: I.W. Sutherland (Ed.), The Surface Carbohydrates of Prokaryotes, Academic Press, London, 1977, pp. 357–414.
[45] P. Messner, U.B. Sleytr, in: I.C. Hancock, I.R. Poxton (Eds.), Bacterial Cell Surface Techniques, Wiley, Chichester, UK, 1988, p. 97.
[46] H.H.M. Rijnaarts, W. Norde, J. Lyklema, A.J.B. Zehnder, Colloid. Surf. B 4 (1995) 191.
[47] T.W. Healy, L.R. White, Adv. Colloid Interf. Sci. 9 (1978) 303.
[48] R.J. Hunter, Zeta Potential in Colloid Science, Academic Press, London, 1981.
[49] Y.-I. Chang, C.-Y. Hsieh, Colloid. Surf. 53 (1991) 21.

[50] M.K. Yelloji Rao, P. Somasundaran, K.M. Schilling, R. Carson, K.P. Ananthapadmanabhan, Colloid. Surf. B 4 (1995) 87.
[51] R. Bos, H.C. van der Mei, J. de Vries, H.J. Busscher, Colloid. Surf. B 7 (1996) 101.
[52] Z. Adamczyk, P. Warszýnski, Adv. Colloid Interf. Sci. 63 (1996) 41.
[53] B.W. Ninham, V.A. Parsegian, J. Theoret. Biol. 31 (1971) 405.
[54] H. Ohshima, Adv. Colloid Interf. Sci. 62 (1995) 189.
[55] H. Morisaki, S. Nagai, H. Ohshima, E. Ikemoto, K. Kogure, Microbiology 145 (1999) 2797.
[56] J. Kijlstra, R.A.J. Wegh, H.P. van Leeuwen, J. Electroanal. Chem. 366 (1994) 37.
[57] A.M. James, in: N. Mozes, P.S. Handley, H.J. Busscher, P.G. Rouxhet (Eds.), Microbial Cell Surface Analysis, VCH, New York, 1991, p. 221.
[58] M. Von Smoluchowski, Z. Phys. Chem. 92 (1918) 129.
[59] J. Lyklema, Colloid. Surf. 92 (1994) 41.
[60] H.J. Busscher, W. Norde, J. Biomed. Mater. Res. 50 (2000) 463.
[61] H. Ohshima, T. Kondo, Biophys. Chem. 39 (1991) 191.
[62] M.A. Cohen Stuart, F.H.W.H. Waajen, T. Cosgrove, B. Vincent, T.L. Crowley, Macromolecules 17 (1984) 1825.
[63] H.C. van der Mei, J. de Vries, H.J. Busscher, Surf. Sci. Rep. 39 (2000) 1.
[64] C.J.P. Boonaert, P.G. Rouxhet, Appl. Environ. Microbiol. 66 (2000) 2548.
[65] P.N. Dengis, P.G. Rouxhet, Yeast 13 (1997) 931.
[66] H.C. van der Mei, J.M. Meinders, H.J. Busscher, Microbiology 140 (1994) 3413.
[67] H.C. van der Mei, H.J. Busscher, R. Bos, J. de Vries, C.J.P. Boonaert, Y.F. Dufrêne, Biophys. J. 78 (2000) 2668.
[68] A.C.C. Plette, W.H. van Riemsdijk, M.F. Benedetti, A. van der Wal, J. Colloid Interf. Sci. 173 (1995) 354.
[69] M. Fletcher, J. Bacteriol. 170 (1988) 2027.
[70] Y.E. Collins, G. Stotzky, Appl. Environ. Microbiol. 58 (1992) 1592.
[71] C.J. Daughney, J.B. Fein, J. Colloid Interf. Sci. 198 (1998) 53.
[72] E. Wasserman, A.R. Felmy, Appl. Environ. Microbiol. 64 (1998) 2295.
[73] H.H.P. Fang, K.-Y. Chan, L.-C. Xu, J. Microbiol. Meth. 40 (2000) 89.
[74] P.J.M. Kiers, R. Bos, H.C. van der Mei, H.J. Busscher, Microbiology 147 (2001) 757.
[75] S. Takashima, H. Morisaki, Colloid. Surf. B 9 (1997) 205.
[76] E.L. Carstensen, R.E. Marquis, Biophys. J. 8 (1968) 536.
[77] J. Lyklema, H.P. van Leeuwen, M. Minor, Adv. Colloid Interf. Sci. 83 (1999) 33.
[78] S.S. Dukhin, J. Lyklema, Langmuir 3 (1987) 94.
[79] A. van der Wal, M. Minor, W. Norde, A.J.B. Zehnder, J. Lyklema, J. Colloid Interf. Sci. 186 (1997) 71.
[80] J.M. Meinders, H.C. van der Mei, H.J. Busscher, J. Colloid Interf. Sci. 164 (1994) 355.
[81] D.Y.C. Chan, D.J. Mitchell, J. Colloid Interf. Sci. 95 (1983) 193.
[82] H. Ohshima, K. Makino, T. Kondo, J. Colloid Interf. Sci. 116 (1987) 196.
[83] J. Visser, in: Matijevic (Ed.), Surface and Colloid Science, Vol. 8, Wiley, New York, 1976, p. 3.
[84] H. Ohshima, T. Kondo, J. Colloid Interf. Sci. 157 (1993) 504.
[85] H.-K. Tsao, Y.-J. Sheng, Langmuir 14 (1998) 6793.
[86] H.-K. Tsao, J. Colloid Interf. Sci. 205 (1998) 538.
[87] S.H. Behrens, M. Borkovec, J. Phys. Chem. B 103 (1999) 2918.
[88] M. Elimelech, C.R. O'Melia, Langmuir 6 (1990) 1153.
[89] M.L. Grant, D.A. Saville, J. Colloid Interf. Sci. 171 (1995) 35.
[90] M.C.M. van Loosdrecht, J. Lyklema, W. Norde, G. Schraa, A.J.B. Zehnder, Appl. Environ. Microbiol. 53 (1987) 1893.
[91] A. Zita, M. Hermansson, Appl. Environ. Microbiol. 60 (1994) 3041.
[92] D.G. Jewett, T.A. Hilbert, B.E. Logan, R.G. Arnold, R.C. Bales, Water Res. 29 (1995) 1673.
[93] J.M. Meinders, H.C. van der Mei, H.J. Busscher, J. Colloid Interf. Sci. 176 (1995) 329.
[94] H.C. van der Mei, P. Brokke, J. Dankert, J. Feijen, H.J. Busscher, J. Disp. Sci. Technol. 13 (1992) 447.
[95] B. Gottenbos, H.C. van der Mei, H.J. Busscher, D.W. Grijpma, J. Feijen, J. Mater. Sci.: Mater. Med. 10 (1999) 853.
[96] H. Morisaki, K. Nakagawa, H. Shiraishi, Colloid. Surf. B 6 (1996) 347.
[97] A.T. Poortinga, R. Bos, H.J. Busscher, Langmuir 17 (2001) 2851.
[98] H.H.M. Rijnaarts, W. Norde, E.J. Bouwer, J. Lyklema, A.J.B. Zehnder, Environ. Sci. Technol. 30 (1996) 2877.

[99] B.F. Smets, D. Grasso, M.A. Engwall, B.J. Machinist, Colloid. Surf. B 14 (1999) 121.
[100] M.M. Cowan, F.H.M. Mikx, H.J. Busscher, Colloid. Surf. B 2 (1994) 407.
[101] M.C.M. van Loosdrecht, J. Lyklema, W. Norde, G. Schraa, A.J.B. Zehnder, Appl. Environ. Microbiol. 53 (1987) 1898.
[102] J. Israelachvili, Intermolecular and Surface Forces, Academic Press, London, 1992.
[103] B.A. Jucker, H. Harms, S.J. Hug, A.J.B. Zehnder, Colloid. Surf. B 9 (1997) 331.
[104] B.A. Jucker, A.J.B. Zehnder, H. Harms, Environ. Sci. Technol. 32 (1998) 2909.
[105] S. Biggs, Langmuir 11 (1995) 156.